Environmental Forensics, 4:47–62, 2003

1527–5922/03 $12.00 + .00
DOI: 10.1080/15275920390186976

Taylor & Francis
Taylor & Francis Group

Perched Water Bodies in Arid Environments and Their Role as Hydrologic Constraints for Recharge Rate Estimation: Part 2. The Case of Yucca Mountain

Amvrossios C. Bagtzoglou

Department of Civil and Environmental Engineering, University of Connecticut, Storrs, CT, USA

The formation and temporal evolution of perched water bodies in the Yucca Mountain (YM) site is the focus of this article. Following the approach proposed by Bagtzoglou (2003), recharge rates that would be required to form and sustain perched water bodies with characteristics similar to the known occurrences at YM are estimated through a series of detailed flow simulations. The results were tested for plausibility by comparing with hydrological and geochemical data. The proposed approach is applied with reasonable discriminatory success to a specific geologic cross-section at the YM site, and recharge rates of 0.13, 0.51, and 6.2 mm/yr are calculated for a set of three hydraulic property realizations. However, only the highest recharge rate (6.2 mm/yr) satisfies both hydrological and geochemical constraints. This is in excellent agreement with current estimates by the US Department of Energy.

Keywords: Yucca Mountain, infiltration, hydrologic modeling, recharge, perched water.

Introduction

Yucca Mountain (YM) in southern Nevada is being considered by the US Department of Energy (DOE) as a potential site for the long-term storage of high level nuclear waste. This site has been selected as a candidate high level waste (HLW) repository site because: (1) it is situated in a remote location; (2) the general area is characterized by a low population density; and (3) it is characterized by an up to 700 m thick unsaturated zone (US DOE, 1986). Thus, the proposed repository, at a depth of approximately 300 to 400 m, is considered to be well protected from processes occurring at the surface and the water table. The favorable geochemical and hydrologic environment provided by the unsaturated zone suggests that high fluxes of water may not readily penetrate the repository, thereby keeping at a minimum waste-package degradation rates and release of dissolved spent fuel.

Parts of the repository being located in a localized saturated zone would mean an increase in the rate of corrosion of the containers and dissolution of the radioactive waste. Even if the repository itself were not actually in the saturated zone, a perched water zone nearby could mean accelerated transport rate of radionuclides into the environment in the event of canister failure. This is particularly important since the host rock (i.e., the geologic unit within which the repository is planned to be constructed) is highly fractured. It is well recognized that under saturated—and, under special circumstances, unsaturated—conditions fractures within tuffs similar to those that occur at YM exhibit very fast response times, capable of conveying amounts of water multiple orders of magnitude greater than that, which can be conveyed by the matrix.

The potential for formation of perched water bodies is identified in federal regulations, for example 10 CFR 60.122(c)(23), as a potentially adverse condition for the storage of HLW in a geologic repository. Perched water is common in arid environments. For example, perched water flows from seeps into the U12n tunnel through the zeolitized Indian Trail Tuff at Rainier Mesa, 50 km northwest of YM (Thordarson, 1965; Russell et al., 1987; Wang et al., 1993). Isotopic signatures (δD and δ^{18}O) indicate that the perched waters at Rainier Mesa are similar to modern meteoric waters and result from recharge relatively quickly from local winter precipitation (Russell et al., 1987). Evidence also suggests that waters from the seeps in the zeolitized tuffs are chemically similar to water from the unsaturated zone below the perched water body, but are distinct from shallower waters (Wang et al., 1993).

Perched water bodies tend to be long-term transient features that are formed where there is a contrast in hydrologic properties (Freeze and Cherry, 1979). Contrasts may result from differences between stratigraphic units. For example, hydraulic conductivity at YM tends to decrease with increased welding of the tuff units. Contrasts may also occur due to the juxtaposition of low-conductivity strata adjacent to more permeable and conductive strata along a structural feature such as a fault or other persistent discontinuity. YM is criss-crossed by numerous potentially permeable faults, as can be seen in Figure 1, thus substantially increasing the probability of locally saturated conditions occurring

Received 3 April 2002; accepted 19 July 2002.
Address correspondence to Amvrossios C. Bagtzoglou, Department of Civil and Environmental Engineering, University of Connecticut, 261 Glenbrook Road, Unit 2037, Storrs, CT 06269-2037, USA. E-mail: acb@engr.uconn.edu

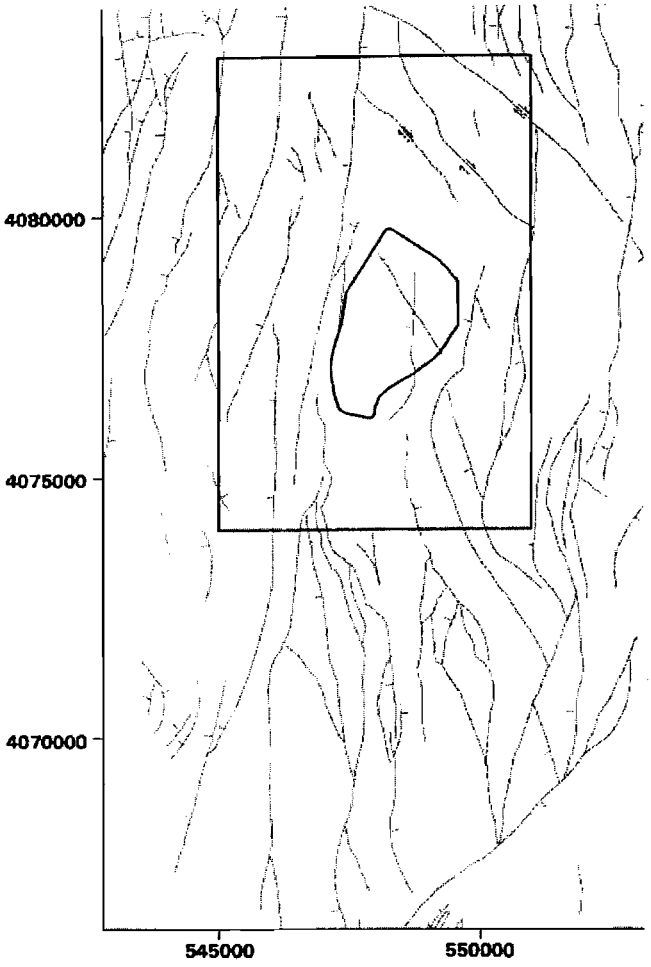

Figure 1. Major faults present in the YM site, as identified in the geologic map by Frizzell and Shulters (1990). The image inner window covers coordinates that range from 545,000 to 551,000 in the x-direction and from 4,074,000 to 4,082,000 in the y-direction. Note that the outline of the proposed repository, indicated in thick solid line, is outdated and is depicted only for georeferencing purposes.

based on the conceptual model presented in the first part of this paper (Bagtzoglou, 2003).

At YM, smectite content increases towards the north; this is likely due to hydrothermal alteration that was associated with the Timber Mountain Caldera (Bish and Aronson, 1993) north of YM. Smectite content also varies with depth, with higher smectite concentrations occurring in fractured, welded tuff (high permeability) above bedded, nonwelded tuff (low permeability). Trends in mineralogy of this type point to areas of focused hydrothermal flow, and help to delineate paleohydrology. High concentrations of clays such as smectite may also serve to create low permeability zones that are favorable to the formation of perched water zones. This may be particularly enhanced at YM, where both higher smectite contents and higher infiltration rates (Flint and Flint, 1994) are found in the northern part of the site.

If perched water bodies formed above the repository, this local saturation could induce localized fracture flow along vertical pathways downward into the repository. Past (and contemporary) occurrence of fracture flow that bypassed part of the unsaturated zone where matrix flow would normally predominate, thus transporting released contaminants at greater flow rates, has been recently inferred by ^{36}Cl measurements at the Exploratory Studies Facility (ESF), within the repository host rock at YM (Fabryka-Martin et al., 1996). Bomb-pulse ^{36}Cl has been identified at a few very distinct, highly fractured zones, generally in the vicinity of faults, indicating that a small amount of water at these locations is less than 50 years old and that it was, most probably, transported preferentially through extremely localized pathways. However, there exists no evidence that these fast pathways are indeed associated with a perched water body that induced this flow pattern in the past.

Although they do exist now, perched aquifers would be more likely to form or expand under wetter, climatic conditions that cause increased recharge flux. Such conditions have existed in the past (i.e., the Pleistocene), and it is possible that perched aquifers at the YM area are relict features formed by higher infiltration rates during former pluvial climates. Perched aquifers may also form where alluvial deposits underlie intermittent stream channels. When ephemeral stream flow saturates the alluvial material, the alluvium may remain saturated long after the stream channel is dry. Even though these perched aquifers would be located near the surface, the water could eventually drain through fractures to the water table below. More importantly, it is possible that water from these perched aquifers could find its way into the host rock by vertical and lateral flow along contacts at or near locations where the repository host rock is exposed. Perched aquifers in alluvial material at YM may be difficult to identify because they are probably infrequent and of short duration. However, like intermittent streams, they have the potential to form, drain, and form again.

Hydrogeologic Setting

The YM site is located approximately 160 kilometers northwest of Las Vegas, Nevada. It is composed of layers of Tertiary volcanic tuff and consists of a series of north-trending fault-block ridges that are generally slightly dipping to the southeast (5° to 10°). The region is in the tectonically active Basin and Range Province, and a number of extensional faults are present within a few kilometers of the proposed repository footprint. Rock units range from densely welded and highly fractured tuffs to less-fractured, nonwelded and moderately welded units. Surficial units are deeply incised with washes, particularly on the eastern flank of the YM ridge. A thin coating of alluvium/colluvium covers much of YM, achieving depths of tens of meters in some of the larger washes. A detailed description of the geologic and hydrologic setting of the YM site follows.

Basin and Range Province

The Basin and Range province extends from southern Idaho and Oregon, where it is bounded on the north by the Columbia

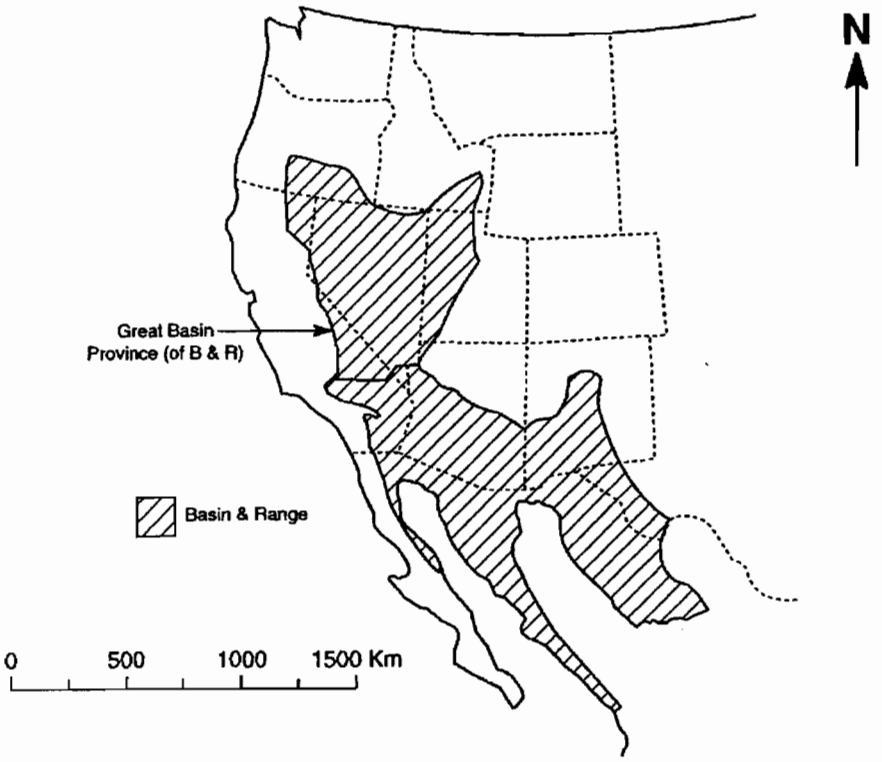

Figure 2. The Basin and Range province and its northernmost section, the Great Basin.

Plateau, 1500 km southward to northern Mexico, where it is bounded on the south by the Sierra Madre (Figure 2). The Basin and Range province has a long and complex geologic history, beginning in the Precambrian and extending into the Holocene. Structures that were produced by more recent geologic events may reflect the influence of an even earlier structural feature (Stewart, 1984). For example, the trend of the current geologic features follows the trends of geologic features produced by earlier geologic events. Plate collisions accreted much of this region onto the then continental margin of the prePaleozoic and Paleozoic North America. Late Paleozoic and Mesozoic events later modified this region. Early Mesozoic subduction of the Kula plate beneath the North American plate produced an Andean-style volcanic range with large scale granitic igneous intrusions that was later exposed to become what we know as the Sierra Nevada batholith. Areas further inland were relatively unaffected by this subduction at that time. A later increased rate of subduction (caused by an increase in Atlantic seafloor spreading rate) did produce structural changes in the Great Basin region, including folding and thrusting along a well-defined belt from Canada to Mexico. This deformation occurred primarily during the Sevier (late Jurassic to late Cretaceous) and Laramide (late Cretaceous to middle or later Eocene) orogenic events and thrust late prePaleozoic and early Paleozoic rocks over late Paleozoic and Mesozoic rocks (Fiero, 1986).

YM is in the Basin and Range province, and more specifically the Great Basin section of the Basin and Range province. The Basin and Range province is divided into five sections, and the Great Basin is the northernmost section (Dohrenwend, 1987). It ranges from southern Idaho and Oregon through most of Nevada and much of western Utah and eastern California (Figure 2). It borders the Colorado Plateau and the middle Rocky Mountains on the east and northeast, respectively, and the Sierra Nevada and the Cascade Range on the west and northwest, respectively, and the Garlock Fault zone to the south. The Great Basin is not, as its name suggests, a large basin; rather it is an elevated region that contains many sub-basins and is flanked on three sides by lower terrain: (1) Bonneville basin on the east, (2) Lahonton basin on the west, and (3) on the south a less well-defined lowland region comprising much of southern Nevada. Except for certain regions in the north, northwest and southeast, all the sub-basins in the Great Basin are closed. In the early to middle Cenozoic, extreme eruptions of silicic volcanic material occurred in the Great Basin region. Igneous activity migrated generally southward during the early to middle Cenozoic; from Washington about 45–59 million years before present (maBP) to central Idaho and northwestern Wyoming about 38–49 maBP, to northern Nevada about 43–33 maBP, and finally to central Utah about 20–34 maBP (Stewart, 1984). While early and middle Cenozoic volcanic activity was widespread over most of the Great Basin, late Cenozoic igneous activity occurred primarily along the margins of the Great Basin

(Stewart, 1984). Alternating layers of welded and nonwelded tuff occur in the vicinity of YM and can typically be traced laterally throughout the area. These layers vary in thickness from tens to hundreds of meters with the major welded ashflow tuffs being usually separated by thinner intervals of nonwelded to poorly welded ashfall and airfall tuffs and reworked tuffaceous material (Wilson et al., 1994). At about 13 to 14 maBP, eruptions from Claim-Canyon cauldron, Timber Mountain-Oasis Valley caldera complex, Wahmonie area, and Crater-Prospector Pass caldera complex produced thick ash flow and airfall tuff that occur in the area of this study (Byers et al., 1989). These layers correspond to eruptions that relate to the collapse of caldera systems (Wilson et al., 1994).

The present structural and geomorphic character of the Basin and Range is a product mainly of the late Cenozoic tensional stresses to which it has been subjected, beginning about 17 maBP. This has produced extension in the region, with most estimates for this extension in the range of between 10% and 35% of the original width of the province (Stewart, 1984). Along with this extension was a regional uplift of as much as about 2,000 m. This extension is manifest in this area by anomalously high heat flow, low upper mantle seismic velocity, low regional gravity field values, and an extensive series of normal faults. The trend of this faulting generally follows previous geologic structural patterns. The northern part of the Great Basin with its well defined, steep, parallel, linear range fronts is contrasted with the southern portion where, along a well-defined east-west line, the character of the topography goes to a more mature terrain, with lower mountains with wide surrounding complexes of pediments and alluvial fans. Fresh fault scarps and active seismicity are uncommon in the southern portion. Whereas the northern portion appears to be a tectonic province of active uplift and extension, the southern region appears to be nearly seismically stable. The tensional forces are generally east-west oriented, producing normal faults that strike roughly north-south. This north-south normal faulting often produces a series of linear north-south trending upthrown blocks (horst) and downthrown blocks (grabens) (Figure 3). The throw of these faults is typically about 2,000 to 5,000 m in the Great Basin region. This large amount of structural relief is typically masked by accumulations of sediment with a thickness ranging from a few hundred meters to more than 3,000 m (Stewart, 1984). Another important way of producing common Basin and Range structures is by the tilting of the structural blocks along listric normal faults (faults that decrease in their dip angle as their depth increases). The product of this

Figure 3. Horst and graben structures; the downthrown and upthrown blocks form the grabens and horsts, respectively.

Figure 4. Fault block structures become inclined as they move downward along listric normal faults.

tilting along a listric fault is that the upslope portion of the tilted block forms the ridge and the downslope part forms the valley (Figure 4).

Local Geologic Setting

YM is located at the western edge of the Nevada Test site about 150 kilometers northwest of Las Vegas, Nevada (Figure 5). It is a rather narrow ridge that formed as a result of being the upthrown block relative to the downthrown blocks on either side of it. It trends roughly north-south and is tilted between 5 to 10° to the south-southeast. The western edge is bounded by the Solitario Canyon Fault, and just west of the fault is Solitario Canyon, which is about 180 m lower in elevation than the crest. The eastern side is dissected by a series of washes running east to southeast toward Jackass Flats, which is about 460 m below the crest. YM is also cut, primarily in the east, by a series of mostly north-south striking normal faults, which are upthrown to the east. Between this series of faults on the east, the Solitario Canyon Fault on the west, and the right lateral strikeslip shear zone in Drill Hole Wash to the northeast, exists a roughly triangular region that is relatively less complex structurally than the surrounding area. This region is known as the central block of

Figure 5. Location of Yucca Mountain, the site of the proposed high-level nuclear waste repository in southern Nevada.

YM. Two significant faults run through the central block. These faults are the nearly vertical Ghost Dance normal Fault, which strikes north-south, and the right lateral Sundance Fault, which strikes, northwest-southeast.

YM is composed primarily of volcanic tuffs of Miocene age. The tuff layers range from densely welded and highly fractured to less fractured and nonwelded to moderately welded. A thin cover of alluvium/colluvium overlies most of YM, and in some of the larger washes it accumulates to depths of tens of meters. Three formations occur in the unsaturated zone of YM. These are, in ascending stratigraphic order, Crater Flat Tuff, tuffaceous beds of the Calico Hills, and the Paintbrush Tuff. Hydraulic properties of the rocks are related more to their physical characteristics, which are largely dependent upon the degree of welding, than to their petrographic characteristics. Hydraulic boundaries based on physical properties (due to the degree of welding) do not necessarily correspond to boundaries based on petrographic characteristics. The tuffs are variably fractured and although the more densely welded tuffs have a lower porosity, they are generally more densely fractured. The Center for Nuclear Waste Regulatory Analyses (CNWRA) staff has grouped the rocks according to hydrogeologic properties. The names and descriptions of the rock unit divisions are given in Stirewalt et al. (1994) and discussed below. The Tiva Canyon Member of the Paintbrush Tuff is moderately to densely welded and comprises the *Tiva Canyon welded Tuff*. Undifferentiated formations of the upper Paintbrush Tuff and part of the lower Tiva Canyon Member are nonwelded to partially welded tuffs and comprise the *Paintbrush nonwelded Tuff*. The Topopah Spring Member of the Paintbrush Tuff comprises the *Topopah Spring1, 2, 3 welded Tuffs*. The upper portion of this member is composed of moderately to densely welded, lithophysae-rich ashfall tuffs. The lower portion is composed of moderately to densely welded, lithophysae-poor ashfall tuffs and a basal vitrophyre. This study considers the Topopah Spring1, 2, 3 welded Tuffs as one stratum. Undifferentiated Calico Hills Tuffs, lower Paintbrush Tuff and Upper Crater Flat Tuff are nonwelded ashfall and bedded tuffs, and these comprise the *Calico Hills nonwelded Tuff*. The moderately welded ashfall tuffs of the Prow Pass Member of the Crater Flat Tuff form the *Prow Pass welded Tuff*. Undifferentiated Upper Crater Flat Tuffs, including the Lower Prow Pass and the Upper Bullfrog Member, form the *Crater Flat undifferentiated nonwelded Tuff*. These members are zeolitic and nonwelded to partially welded ashfall and bedded tuffs. The Bullfrog Member of the Crater Flat Tuff is moderately to densely welded ashfall tuffs and forms the *Bullfrog welded Tuff*. The repository is intended to be positioned deep within the relatively dry, unsaturated Topopah Spring welded Tuff, about 300–400 m below the ground surface and approximately 250 m above the water table (US DOE, 1988).

In addition to the presence of markedly distinct geologic units and tectonic faults, the geologic units are also variably fractured. For example, the Topopah Spring welded unit, where the proposed repository is to be located, is a low-porosity welded tuff believed to be densely fractured, while the underlying Calico Hills, nonwelded-vitric or zeolitized unit is a higher porosity, nonwelded tuff with seemingly much lower fracture density (US DOE, 1988).

Climate

This region has currently an arid climate and receives a mean annual rainfall of about 150 mm/yr, nearly 75% of which occurs from October through April as frontal systems move through the region. Warm season precipitation usually occurs as brief, intense thunderstorms. Many relict landforms and sedimentary deposits in the Basin and Range province indicate a previous climate that was much different than today. For example, cirques, nivation hollows, and glacial moraines are found, as are fluvial and beach deposits. From a relatively noisy background of tectonic, lithologic, and evolutionary influences, the influences of climatic change are difficult to filter out. Many studies have been conducted on the paleoclimate of the American Southwest, but the results are usually only in partial agreement or even directly contradictory. For example, full-glacial conditions from different studies range from cold and dry to mild and wet. Estimates of full-glacial mean annual temperature range from 2.8 to 16°C colder than present, and full-glacial mean annual precipitation estimates range from 50% to approximately 200% of present levels. Although some of this variation can certainly be attributed to different approaches and assumptions, a substantial part of the differences is almost certainly due to the specific areas of the different studies being affected differently, both in magnitude and in character, by the changing regional climate. Some basic characteristics of this regional climatic change, however, do seem to be constant throughout most of the region. For example, during the period between about 25 and 12 thousand years before present (kaBP) pluvial lake levels were high to intermediate, after which time they declined rapidly and were low to dry between approximately 10 to 5 kaBP. Furthermore, pinyon-juniper woodlands were present at approximately the same time as the high lake levels in areas where now only desert scrub communities exist. Finally, the effective moisture of the latest Pleistocene and the earliest Holocene was significantly greater than the present-day effective moisture.

Spaulding (1985) conducted research with plant microfossils and dated remains found in packrat middens in the vicinity of the Nevada Test site. Based on this work, Spaulding (1985) reported that the climatic conditions at the Nevada Test site about 45 kaBP were very similar to the present-day conditions in northern Nevada. Figure 6 summarizes precipitation and temperature changes for a base, an upper bound, and a lower bound case for the past 45,000 years near the Nevada Test site as inferred by analyzing original data reported in Spaulding (1985). Three distinct precipitation and temperature regimes can be identified: (1) 45 to 39 kaBP is a period of decreased temperature when precipitation increased from present levels to 15% greater than present; (2) 38 to 18 kaBP is a period when precipitation varied from 16 to 40% greater than present, with temperatures from 3–6°C cooler than present; and (3) a definite warming period

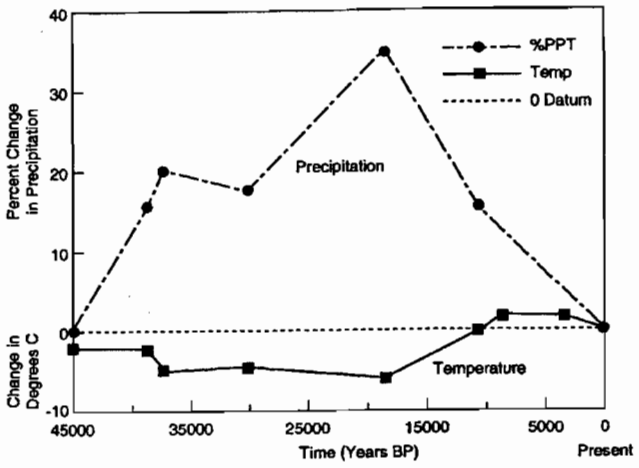

Figure 6. Precipitation and temperature changes from present conditions for the past 45,000 years in the vicinity of the NTS. Based on original data from Spaulding (1985).

from 18 to 13 kaBP to present, in which precipitation declined back to present-day levels while temperature increased by 4°C. The lower temperature and greater precipitation of the past pluvial climate that are shown in Figure 6 indicate that a significantly greater infiltration and groundwater recharge probably occurred during that time. Even though it is fair to speculate that most of this recharge occurred in the areas of higher elevation north of YM, it is hypothesized that water was also able to find its way down in the area of the proposed repository more rapidly and in greater quanities than at present. Calcite deposits that are thought to have been formed from the main aquifer exist above the present water table. This suggests that the water table has been higher in the YM region than it is today by approximately 115 m (Quade and Mifflin, 1995). Qualitatively similar observations were made by Geyh et al. (1995) for the Nubian sandstone near the river Nile, which has been estimated to have fallen in stages approximately 60 m since the climate changed from a prolonged pluvial period to an arid one (about 6 to 4 kaBP). Czarnecki (1985), following a numerical modeling approach, investigated the effects a wetter future climate would have on the water table and concluded that a 100% increase in precipitation could cause the water table at YM to rise by as much as 130 m. Such a rise in the water table would not be adequate to inundate the repository, located 250–300 m above the current water table, but saturation levels above the higher water table would see an increase from present-day values.

Finally, the net annual infiltration from rainfall and surface water over YM has not been definitively determined yet, but several estimates do exist. They vary from 3.0 to 35.0 mm/yr with an average of 14 mm/yr (Stothoff et al., 1995; Stothoff, 1997), to 2.0 to 20 mm/yr with an average of 5 mm/yr (Bodvarsson et al., 1999), from a mean annual rainfall of about 150 mm/yr. These mean values do not take into account the more extreme rainfall rates that may occur due to interannual and interseasonal fluctuations and individual storms. In addition, these values only reflect contemporary rainfall and infiltration conditions. Under ambient conditions, it is likely that radionuclides released from the repository zone will be transported predominantly in the unsaturated flow regime. However, locally saturated flow conditions may also occur in the vadose zone, possibly due to short and intense rainfalls, or due to extremes in climatic fluctuations on larger time scales, or due to repository-induced elevated temperatures (Ofoegbu et al., 1999, 2001; Buscheck et al., 2002).

Review of Shallow Infiltration Studies at Yucca Mountain

The amounts, timing, and locations of infiltration are controlling factors in the movement of groundwater throughout the site and, therefore, control the formation and temporal evolution of perched water bodies. In fractured, unsaturated rock, such as that found at the YM site, occurrence of infrequent, high-intensity rainfall events may modify, perhaps drastically, the subsurface flow regime from the one predicted by assuming that all rainfall events have average intensities. Indeed, the DOE has concluded that the spatial and temporal distribution of infiltration may be the most important factors influencing groundwater flow path development (US DOE, 1992). Deep percolation fluxes are affected by processes active in the near-surface zone, including evaporation, transpiration, liquid water flow, and vapor flow. Each of these processes is governed by several factors. For example, precipitation has been found to vary substantially over the YM region, both spatially and temporally, and winter storms are, in general, more uniform and of longer duration than summer storms (Hevesi et al., 1992a, 1992b, 1994). These observations indicate that, especially for summer storms, a spatially uniform precipitation pattern is clearly not applicable, even at the site scale. Similarly, evaporation from the ground surface is affected by air temperature, atmospheric vapor pressure, wind speed profile, incident solar radiation, surface soil and rock texture, plant activity, surficial temperature, and surficial moisture content.

The sensitivity of long-term net infiltration to each infiltration-affecting factor was first estimated using detailed numerical simulations of the shallow subsurface (Stothoff et al., 1995; Stothoff, 1997). The calculated sensitivity is generic, thus is not dependent on a particular spatial location. Then, each of the infiltration-affecting factors was evaluated on a fine grid over the entire YM area. Potential infiltration-affecting parameters include air temperature, atmospheric vapor pressure, wind speed profile, incident solar radiation, surface soil and rock texture, plant activity, surficial temperature, and surficial moisture content, all of which may vary widely both in space and time. Finally, the calculated sensitivity information was used to estimate net infiltration over the fine grid. The numerical simulator, BREATH (Stothoff, 1995), was used to calculate flow in 1D columns. At the bottom boundary of each column, a zero-saturation-gradient (unit-head-gradient) boundary condition was applied to simulate gravity drainage. At the top boundary of the column, the simulator was presented with 10 years of meteorological inputs on an hourly basis, based on hourly readings from the Desert Rock,

NV, National Weather Service meteorological station located approximately 30 miles to the east of YM (National Climatic Data Center, 1994).

In order to estimate the spatial distribution of infiltration, the YM area was subdivided into three classes: (1) alluvium, (2) fractured welded bedrock overlain by alluvium, and (3) nonwelded bedrock. The alluvium within the Scott and Bonk (1984) outline covers about 31% of the total site area. Based on the CNWRA 3D Geologic Framework Model (GFM) (Stirewalt and Henderson, 1995), welded-tuff bedrock underlies 64% of the remaining area, while nonwelded tuffs are exposed in the remaining 5%. Based on alluvium distributions resulting from nominal source term parameters and corrected with the empirical slope-dependent alluvium depths within the Scott and Bonk (1984) alluvium outline, the infiltration distribution is calculated using the base case alluvium and fracture properties. The average infiltration over the YM site area (6 km E-W × 9.5 km N-S) was found to be 14.0 mm/yr, while within the 3 km E-W × 4.5 km N-S window surrounding the proposed repository footprint the average infiltration was found to be 15.6 mm/yr. In general, the coefficient of variation (CV) for pixel-by-pixel (30 × 30 m) infiltration was found to be larger for the subregional area than for the repository box, suggesting that infiltration patterns are more uniform within the proposed repository footprint than over the region as a whole.

The largest Annual Average Infiltration (AAI) tends to be on sideslopes, whereas in the wash bottoms little or no AAI is predicted. It is plausible to assume that there could be enhanced AAI at the foot of the sideslopes due to overland flow of runoff; there may also be additional AAI within the intermittent stream channels within the washes. The predicted areally averaged AAI rates range from 3 to 45 mm/yr (Figure 7a). As a comparison, USGS estimates of infiltration within the proposed repository footprint were on the order of 25 mm/yr (Flint et al., 1995), and current DOE estimates range from 2 to 20 mm/yr (Bodvarsson et al., 1999). Similar recharge estimates were obtained by Wood and Sanford (1995) for the semiarid Southern High Plains of Texas and New Mexico. Their analysis was based on the chloride mass-balance method and, even though it dealt with completely different materials, average recharge estimates of approximately 11 mm/yr were obtained.

Perched Water Body Occurrences at Yucca Mountain

A number of perched zones have been found at several boreholes (USW UZ-1, UZ-14, NRG-7a, SD-7, and SD-9) at YM (Burger and Scofield, 1994; Yang et al., 1996; Wu et al., 1999). A vacuum-reverse-air-circulation drilling method was used for these boreholes to prevent contamination from drilling fluids, and all perched water samples were collected using plastic or stainless-steel bailers. All perched water found occurs in the upper Calico Hills unit, with the exception of UZ-14 and USW SD-9, where the perched water body is found on the basal vitrophyre in the Topopah Spring unit. Boreholes UZ-1 and UZ-14, which are on the same drilling pad, encountered a perched zone at a depth of 190 m above the water table. The zone was extensive enough to be pump-tested at a rate of 0.204 m^3/h for 67 h, and a total of 22.71 m^3 was produced. It has been estimated, however, that this perched water zone is much more extensive than originally thought, with an approximate volume of 114,000 m^3 (Yang et al., 1996). In USW SD-9, perched water appeared to be just above the basal vitrophyre of the Topopah Spring unit, 120 m above the water table. Boreholes that encountered perched water within the Calico Hills Tuffs include USW SD-7 and USW NRG 7/7a. The perched zone encountered by SD-7 was extensive enough to be pump-tested at a rate of 0.75 m^3/h for 30 h, and a total of 45.42 m^3 was produced. This perched water zone is a relatively small body and its total volume has been estimated at approximately 300 to 500 m^3. Figure 7b depicts the location of all boreholes in the vicinity of the proposed repository (even boreholes that were not studied explicitly for perched water occurrence) together with an outline of the now completed ESF tunnel. Finally, Figure 7c presents a geologic cross-section through all boreholes identified in Figure 7b.

Within 6 to 8 m sampling intervals in the five boreholes large ^{14}C variations are detected, ranging from 27.2 to 66.9 Percent Modern Carbon (PMC) with an average of about 37 PMC, indicating a multitude of water sources that contribute to these perched water reservoirs. The apparent (uncorrected) ^{14}C ages of perched water range from 3,500 to 10,800 years, as indicated by $\delta^{13}C$ data (Yang et al., 1996) accounting for caliche dissolution. The uncertainty in ^{14}C measurements is ± 0.7 PMC (Yang et al., 1996).

Correlation Between Perched Water Occurrences and Shallow Infiltration Distribution at Yucca Mountain

Identifying any association between the nature of potential flow pathways and the evidence of flow based on geochemical and hydrological data is a challenging task. For example, Figure 7a presents a preliminary attempt of correlating the shallow AAI spatial distribution and existing geologic structure with known evidence of perched water occurrence at the YM site. Several observations can be made from this figure. First, there is a reasonable correlation between high AAI values and known perched water occurrences. This is particularly evident when keeping in mind the general southeast dipping trend of the strata, which would force the initially vertical infiltration to be diverted laterally along dip. Second, there appears to exist another important correlation between known perched water occurrences and significant structural features, such as faults or fracture zones. Third, Figures 7a and 7b provide little information to corroborate the link between spatial distribution of AAI, which is estimated at a depth of only 30 m, tectonic features, which may (or may not) cross stratigraphic boundaries, extending upward to the ground surface, and known perched water occurrences at great depths. Existence of such correlations at depth (i.e., where the perched water has been found) would be of great significance because it implies that rapid movement of water from the surface requires discrete, transmissive features extending from

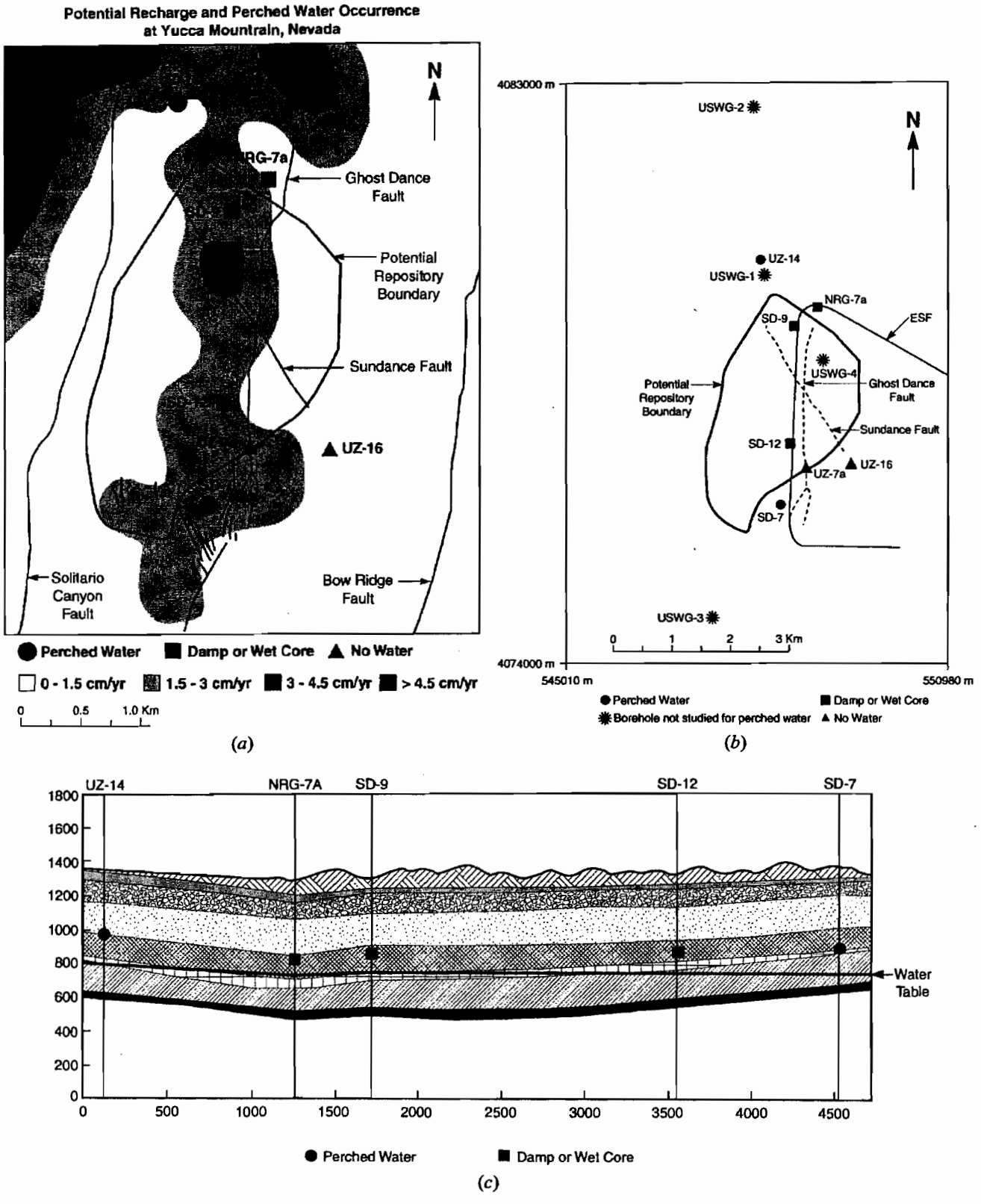

Figure 7. (a) Distribution of smoothed AAI at the YM site, as calculated by Stothoff et al. (1995) at a depth of 30 m, and major faults present. Borehole-associated symbols serve to provide information regarding the occurrence, or not, of a perched water body at each individual borehole. (b) Location of all boreholes in the YM site vicinity, together with ESF outline for georeferencing purposes. (c) Geologic cross-section through YM boreholes. Note that the outline of the proposed repository, indicated in thick solid line, is outdated and is depicted only for georeferencing purposes.

the surface to great depths. Therefore, an effort to provide the missing link and correlate AAI values with known perched water occurrences at depth was deemed necessary.

Perched Water Body Modeling at Yucca Mountain

Faults in YM are common, and this faulting has produced offset of the stratigraphic units. If the offset of the fault is such that a relatively permeable unit within the downthrown fault-block is juxtaposed against a relatively impermeable unit downdip of the fault, then the channeled water will be inhibited from continuing downdip and will eventually become trapped at this location. Therefore, the modeling methodology presented in the first article (Bagtzoglou, 2003) is applicable for the case of YM.

Modeled Area

The first step towards enhancing modeling efforts is to construct a 3D GFM that embodies the current level of understanding of YM by including lithostratigraphy, hydrostratigraphy, and geologic structure (Stirewalt et al., 1994; Stirewalt and Henderson, 1995) of the pertinent region. Lithostratigraphy and geologic structure are based on surface geologic maps of the site (Scott and Bonk, 1984). Subsurface geology is constrained by both borehole control and through the construction of balanced cross sections (Young et al., 1992). Hydrologic properties include porosity, saturated hydraulic conductivity, and water content. For the hydrostratigraphic model, mean values for hydrologic properties are assigned as constant values for each of seven different lithostratigraphic units. Original data are from DOE site characterization activities (e.g., Craig and Reed, 1991; Flint and Flint, 1990; Loscot and Hammermeister, 1992; Whitfield et al., 1993).

The area considered for the current work is the vicinity of the intersection of the Ghost Dance Fault and the Sundance Fault in the repository area of the YM site (Figures 7a and 7b). The modeled area, a 2D cross-section depicted in Figure 8a, is 1100 meters wide by 650 meters deep and is extracted electronically from the GFM. The plane of view is the plane of the Sundance Fault facing northward. The area of interest is above the water table and primarily updip of the Ghost Dance Fault. The right border of this model represents an artificial no-flow boundary that causes water to accumulate, whereas in reality the water would continue flowing downdip past this boundary if no fault were present. However, given the abundance of normal faults in the YM area, this condition may be a representative depiction since it corresponds to a periodic boundary condition, namely a fault existing every so many length units. Any perching to the right of the fault is eliminated from subsequent calculations. The tuff beds that we are dealing with are (from top to bottom): (1) Tiva Canyon welded (TCw), (2) Paintbrush Tuff nonwelded (PTn), (3) Topopah Spring welded 1,2,3 (TSw), (4) Calico Hills nonwelded (CHn), and (5) Prow Pass welded (PPw).

The computational grid used in this work is rectangular with a $\Delta x = 20$ m and $\Delta z = 10$ m, and an automatic time stepping is invoked. The left and right boundaries are no-flow, the top boundary is constant flux, and the bottom boundary is a water table condition (Figure 8b).

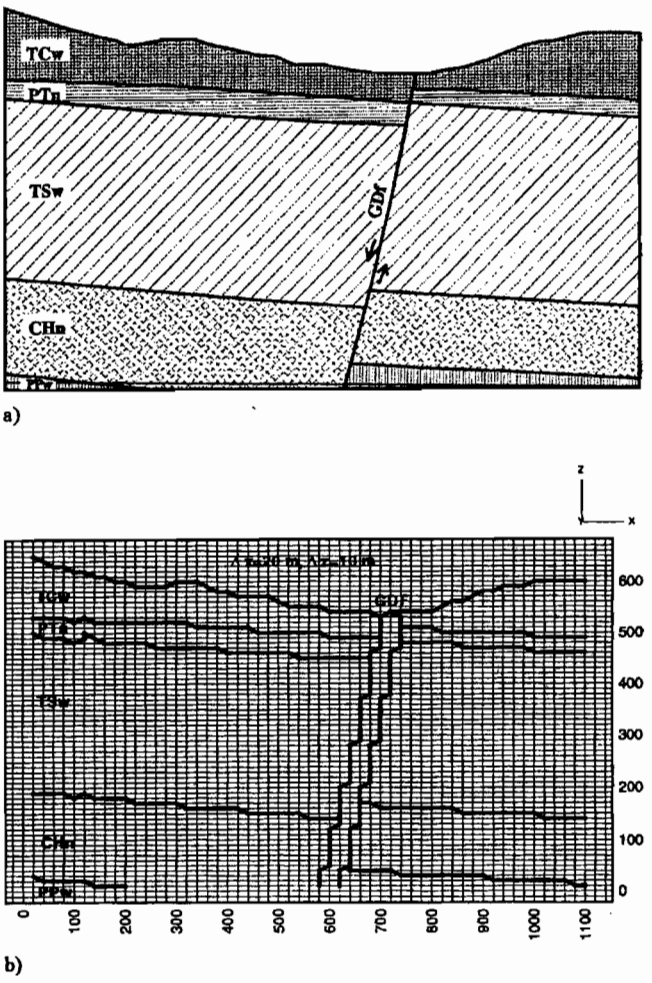

Figure 8. Modeled area. (a) Hydrogeologic units and structural features identified and (b) computational grid used in the simulations. Note that the water table coincides with the bottom boundary and is almost horizontal. TCw, Tiva Canyon welded; PTn, Paintbrush Tuff nonwelded; TSw, Topopah Spring welded; CHn, Calico Hills nonwelded; PPw, Prow Pass welded; GDF, Ghost Dance Fault.

Variability in Hydrologic Properties and Latin Hypercube Sampling

Only limited information is available regarding the spatial variability of hydrologic properties of the volcanic rock units at YM, Nevada. Even though deterministic (geologically controlled) vertical trends in degree of welding within individual units have been identified, insufficient data are available at present to justify using these trends in flow and transport simulations (Istok et al., 1994). Yet, there exists substantial variability in the hydrologic properties, which must be accounted for. Broxton et al. (1993) and Istok et al. (1994) reported coefficients of variation for porosity ranging from 10 to 43%, for permeability ranging from 55 to 75%, and for the logarithm of saturated hydraulic conductivity ranging from 19 to 39%. Ideally, to make the best

final probability estimate for the perching potential, an infinite number of combinations of hydraulic conductivity to saturation level and different saturation levels of different beds should be considered. For each of these combinations the areal extent of the region likely to become perched should be calculated. As discussed in the first part of this paper, in order to obtain sufficiently accurate results without using all possible combinations, a statistical method known as the *Latin Hypercube Sampling* (LHS) was employed to determine the overall probability of the site developing localized perched water zones.

The numerical procedure of estimating the recharge rate that would sustain a perched water body, of specified volume and PMC, can be repeated for as many LHS property set replicates. By calculating statistics on the inferred recharge rate, one could make assertions regarding the variability in this rate and its sensitivity to the hydrologic property variability.

Data

The data used in this study were adopted from the 1993 Total System Performance Assessment (TSPA-1993) for YM (Wilson et al., 1994). Even though it is recognized that there exist more complete data sets, the work presented here is of a methodological and demonstration nature. TSPA-1993 uses 10 hydrogeologic units. Because the GFM model of the YM site used here employs slightly different stratum classifications, some modifications were necessary. Some units are directly equivalent and others were combined by a weighted average based on their relative thicknesses. The Topopah Spring vitrophyre from the TSPA-1993 was not used because it is not continuous over the entire modeled area, and there exists great uncertainty regarding its extent and thickness. The Bullfrog and Tram units were also not used because they lie completely below the main water table in the modeled area. The correlation between the TSPA-1993 division and the current study division are summarized in Table 1.

From the TSPA-1993 data (mean, minimum, maximum, and coefficient of variation), a random sampling of possible values from a beta distribution curve were produced using the LHS approach (Iman and Shortencarier, 1984). The particular data sets used thus far in the study are the mean values, the mean values produced by an entropy-fit procedure, and the third of the fifty random realizations produced by the LHS process. The entropy-fit procedure is used when data are sparse and no physical restrictions exist on the range of the parameters (e.g., porosity must be between 0 and 1). A beta distribution was fitted using a nonlinear optimization entropy-fitting procedure that attempts to use a limited sample to determine properties for an entire population. The values for each of these realizations are listed in Tables 2, 3, and 4. Note that porosity and residual saturation values do not change for these data sets, as there typically exists significantly less uncertainty and spatial variability for the aforementioned parameters. Figure 9 depicts typical results of the 50 LHS-based Monte Carlo realizations for the moisture retention characteristic curve together with the mean value and entropy-fitted mean value characteristic curves.

Table 1. Correlation between TSPA-1993 and current study stratum classification

Unit	TSPA-1993	Unit	Current study
1	Tiva Canyon welded	1	Tiva Canyon welded
2	Paintbrush nonwelded	2	Paintbrush nonwelded
3	Topopah Spring welded	3	Topopah Spring welded
4	Topopah Spring vitrophyre		N/A
5	Calico Hills/Prow Pass nonwelded vitric	4	Calico Hills nonwelded
6	Calico Hill/Prow Pass nonwelded zeolitic		N/A
7	Prow Pass welded	5	Prow Pass welded
8	Bullfrog welded		N/A
9	Bullfrog nonwelded		N/A
10	Tram		N/A

Table 2. Matrix property values taken from TSPA-93 (mean)

Rock unit type	Porosity	K_{sat} (m/s)	Residual saturation	van Genuchten parameters	
				α (m^{-1})	n
TCw	0.087	3.86×10^{-1}	0.021	0.0218	1.622
PTn	0.421	5.470×10^{-7}	0.154	0.2485	2.611
TSw	0.139	2.37×10^{-10}	0.045	0.0299	1.730
CHn	0.319	6.220×10^{-9}	0.113	0.0306	2.087
PPw	0.292	2.580×10^{-9}	0.069	0.0180	7.014

Results and Discussion

The volume of perched water should approach a constant value, V_{pres}, starting from an initial maximum represented by V_{max} in Figure 4 of the first part of this paper, within a time frame that is consistent with the climatic change described in Figure 6, namely 20,000 years. Moreover, the value of PMC for the perched water body, as calculated by Equation (12) of the first part of this paper, should approach a target value, PMC_{pres}, consistent with measurements within the same time period.

The first realization used the mean values from the TSPA-1993. As the system began to drain, with no flux added and an initial uniform head value of -10 m, water began to drain from some areas and accumulate in others. The PTn unit, having a high permeability, allowed water to flow freely down through it.

Table 3. Matrix property values taken from TSPA-93 (entropy-fit mean)

Rock unit type	Porosity	K_{sat} (m/s)	Residual saturation	van Genuchten parameters	
				α (m^{-1})	n
TCw	0.087	2.04×10^{-11}	0.021	0.0079	1.622
PTn	0.421	3.800×10^{-7}	0.154	0.5560	2.371
TSw	0.139	2.09×10^{-11}	0.045	0.0136	1.799
CHn	0.319	3.78×10^{-10}	0.113	0.0133	1.959
PPw	0.292	9.12×10^{-10}	0.069	0.0160	5.888

Table 4. Matrix property values sampled by LHS and using TSPA-93 statistics

Rock unit type	Porosity	K_{sat} (m/s)	Residual saturation	van Genuchten parameters	
				α (m^{-1})	n
TCw	0.087	1.88×10^{-10}	0.021	0.00045	1.393
PTn	0.421	2.21×10^{-7}	0.154	0.21112	1.841
TSw	0.139	1.74×10^{-11}	0.045	0.25927	1.851
CHn	0.319	8.88×10^{-10}	0.113	0.03722	3.539
PPw	0.292	5.48×10^{-9}	0.069	0.0160	5.888

When it encountered the TSw unit, which has a low permeability, its downward flow was inhibited. This caused the water to be channelled downdip in the PTn until it reached the Ghost Dance Fault. The footwall of the fault has been uplifted such that the PTn in the hanging wall is juxtaposed against the relatively impermeable TSw unit in the footwall of the fault. This produces a trap where the water that is channelled downdip through the PTn encounters the relatively impermeable TSw at the fault and begins to accumulate, producing a perched water body. As it continues to accumulate, it percolates slowly downward through the TSw unit, thus extending the perched water body well in the TSw unit. The perched body in the PTn and TSw units continues to grow as long as there is enough water above it to supply it with water faster than it can be dissipated. It reaches a maximum perched water volume of 15,949 m^3 at 455 years (Figure 10), after which the perched water begins to dissipate until it is completely drained by about 1,600 years. Note that a threshold of 99.9% has been applied to the saturation contours in order to make the outline of the perched water body more clear.

Starting from the point in time with maximum perched water volume, a flux was added at the surface to approximate a mean

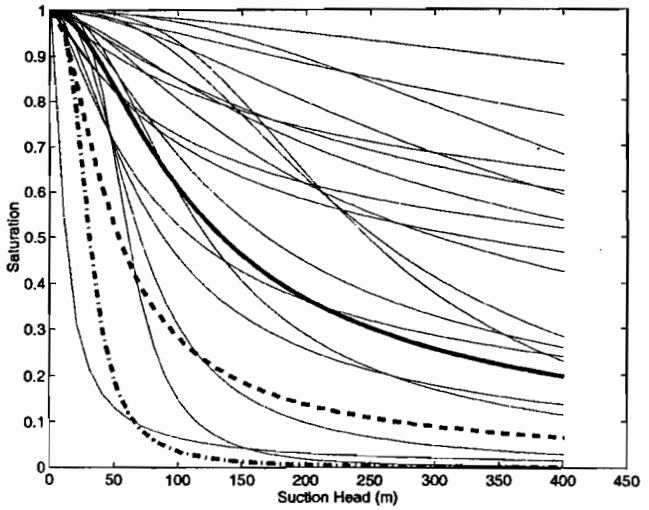

Figure 9. Moisture retention characteristic curves for 50 LHS-generated random realizations (thin solid line), analyzed realization (thick solid line), TSPA-based mean values (thick dash-dotted line), and TSPA-based entropy-fitted mean values (thick dashed line).

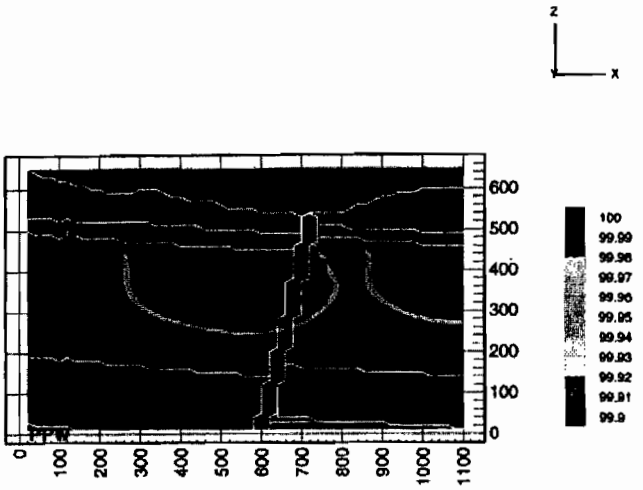

Figure 10. Contour plot of saturation after 455 years of a draining simulation, at which point a maximum perched water volume of 15,949 m^3 has been attained. Note that a threshold of 99.9% is applied to the saturation contours. TCw, Tiva Canyon welded; PTn, Paintbrush Tuff nonwelded; TSw, Topopah Spring welded; CHn, Calico Hills nonwelded; PPw, Prow Pass welded; GDF, Ghost Dance Fault.

infiltration rate. This was allowed to continue until the system reached an equilibrium condition, specifically until the perched water body disappeared or remained at a constant volume. Different flux rates were added until one was found that produced and sustained a perched water body of roughly the same volume of water as actual perched water bodies found in the area (e.g., SD-7), approximately 400 to 500 m^3. In this case, a constant flux of 6.2 mm/year applied uniformly to the top of the system produced a sustained perched water volume of 528 m^3 (Figure 11a) right below the PTn/TSw interface. Figure 11b depicts the exact same saturation field without any threshold application activated; the range of saturation values present throughout this specific cross-section of YM is evident here. Figure 12 depicts the temporal evolution of the perched water volume for the draining simulation, and the simulations with a recharge of 6.2 and 8.0 mm/yr, respectively. Note how the 8.0 mm/yr simulation diverges and floods the system, whereas the 6.2 mm/yr simulation reaches the desired volume asymptotically.

The procedure that used the entropy-fit mean values was used on the realization, and the same general behavior of the water movement was observed. The water drained downward through the more permeable PTn until it encountered the relatively impermeable TSw unit and was channelled downdip until it encountered the TSw unit across the Ghost Dance Fault. At this point the water became trapped and formed a perched water body that expanded downward into the TSw unit. In this realization, however, it proceeded at a much slower rate, and the flux needed to create a sustained perched water body was substantially less than what was required in the previous realization. Under draining conditions, the perched body reached its maximum volume of 8,300 m^3 at about 2,759 years, and by 6,350 years it had completely dissipated. A flux of 0.51 mm/yr produced a sustained perched volume of about 555 m^3 (Figure 13).

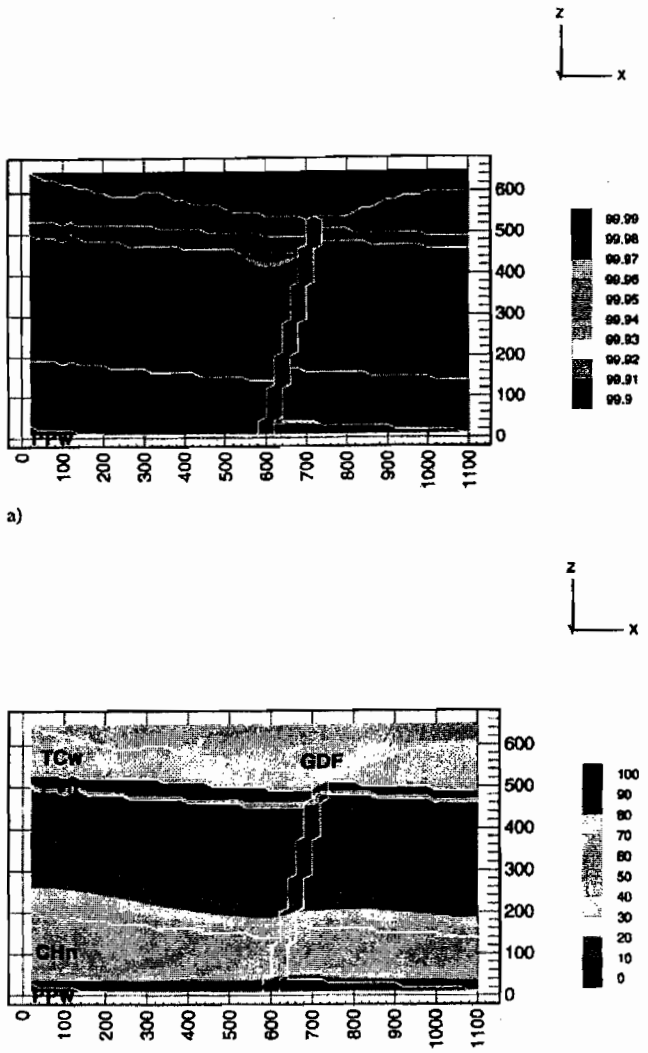

Figure 11. Contour plot of saturation after 455 years of draining and 7,155 years of applying an infiltration rate $q = 6.2$ mm/yr with (a) a threshold of 99.9% applied to the saturation contours and (b) no threshold applied to the saturation contours. TCw, Tiva Canyon welded; PTn, Paintbrush Tuff nonwelded; TSw, Topopah Spring welded; CHn, Calico Hills nonwelded; PPw, Prow Pass welded; GDF, Ghost Dance Fault.

Finally, the same procedure was repeated for one of the 50 LHS-generated random realizations. Because of the properties of the top layer (TCw) and the assumed initial head level of -10 m, this layer was saturated at the very beginning of the simulation and then began to drain. This is the reason for a high initial saturated volume. After this condition disappeared and the saturated volume reached a low of about 926 m^3 at 10 years, the volume began to accumulate again as the water drained from some locations and became trapped in other locations. The maximum volume of 3,676 m^3 was attained at about 8,000 years after the draining began. At about 25,000 years the saturated region had completely dissipated (Figure 14). In the first two realizations, the starting point for all simulations of a

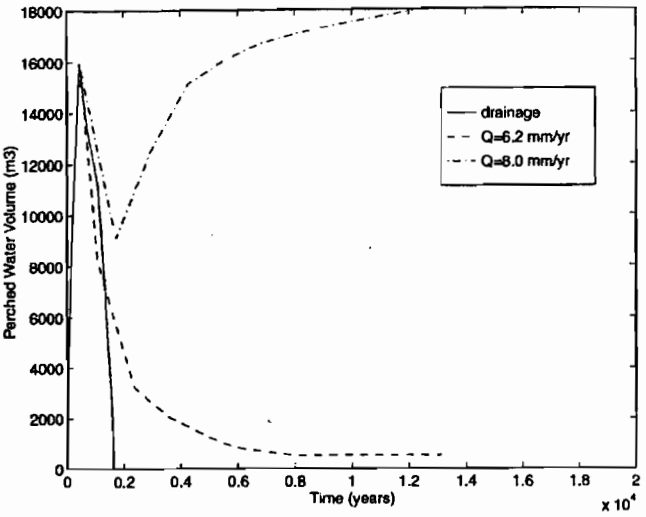

Figure 12. Temporal evolution of perched water volume for draining and $q = 6.2$ and 8.0 mm/yr simulations. Mean TSPA-93 hydrologic properties are used.

specific flux rate subsequent to the draining simulation was the point of maximum perched volume attained during draining. In the LHS-generated realization, however, due to the high initial saturations, two different points further along in the draining simulation were chosen, with an initial volume of 2,530 and 723 m^3, respectively. The results were quite similar (within 2 to 3%) in the final volume of perched water that was calculated in each simulation. The volume of perched water for each simulation reached a final value of approximately 100 m^3 by the end of the simulation.

Several simulations with different flux rates were run for the LHS-generated random realization, to determine which would produce a sustained perched volume of near the target volume

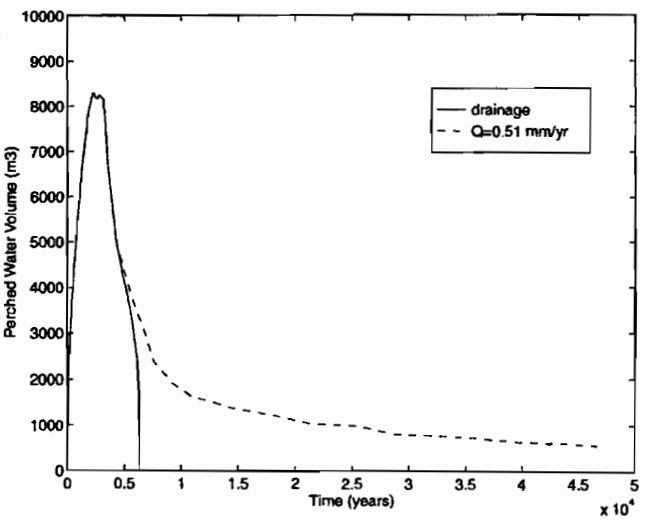

Figure 13. Temporal evolution of perched water volume for draining and $q = 0.51$ mm/yr simulations. Entropy-fit mean TSPA-93 hydrologic properties are used.

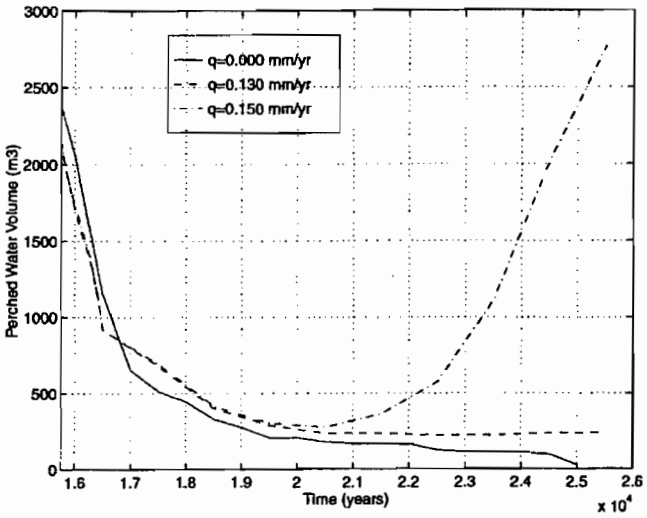

Figure 14. Temporal evolution of perched water volume for draining and $q = 0.13$ and 0.15 mm/yr simulations. LHS-generated hydrologic properties are used.

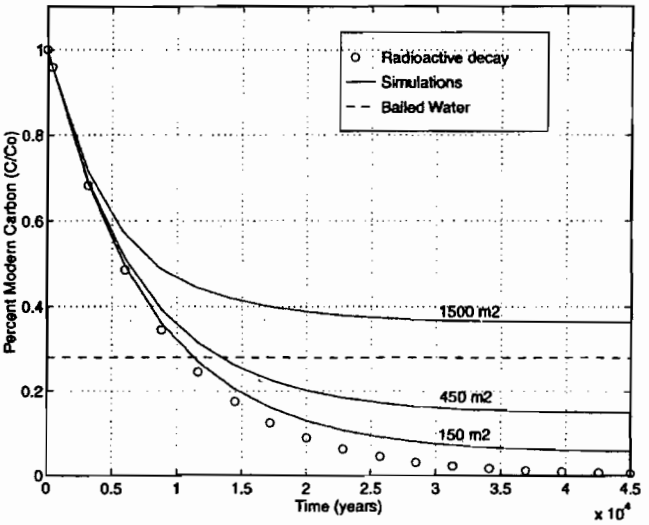

Figure 16. Depletion of perched water ^{14}C as a function of time for $q = 0.51$ mm/yr and three areal extent values. Entropy-fit mean TSPA-93 hydrologic properties are used.

of 400 to 500 m^3. However, for this realization the volumes of perched water did not decrease monotonically to a steady-state value, as was the case for the two previous realizations analyzed (Figure 14). The volume fluctuated with time but with an overall decreasing trend. Fluxes of 0.14 mm/yr and less all produced volumes that fluctuated around values smaller than the target value of 400 m^3 (volume fluctuated from 55 m^3 to about 360 m^3). This made it difficult to determine a specific volume at which it remained for a significant period of time. For the two fluxes greater than 0.14 that were tested, namely 0.15 and 0.20 mm/yr, there was a definite increasing trend in the magnitude of the volume. For this reason these fluxes were considered to not produce a sustained perched volume near the target volume. Although flux rates of 0.12 and 0.13 mm/yr produced volumes less than the target volume, the simulation with 0.13 mm/yr was the largest flux that did not show a strong tendency to increase in value near the end of the simulation. Therefore, this flux rate was chosen for subsequent geochemical analyses (Figure 14).

Equation (12), of the first part of the paper, was solved numerically for each of the three realizations, with input of the $V(t)$ behavior as inferred from the detailed flow simulations. Since the actual areal extent, A, of the perched water body is unknown, simulations have been conducted by varying this parameter. Figures 15, 16, and 17 depict the ^{14}C depletion as a

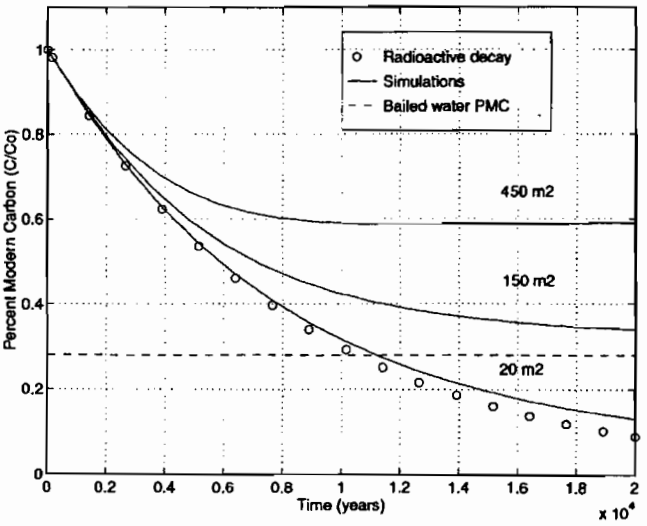

Figure 15. Depletion of perched water ^{14}C as a function of time for $q = 6.2$ mm/yr and three areal extent values. Mean TSPA-93 hydrologic properties are used.

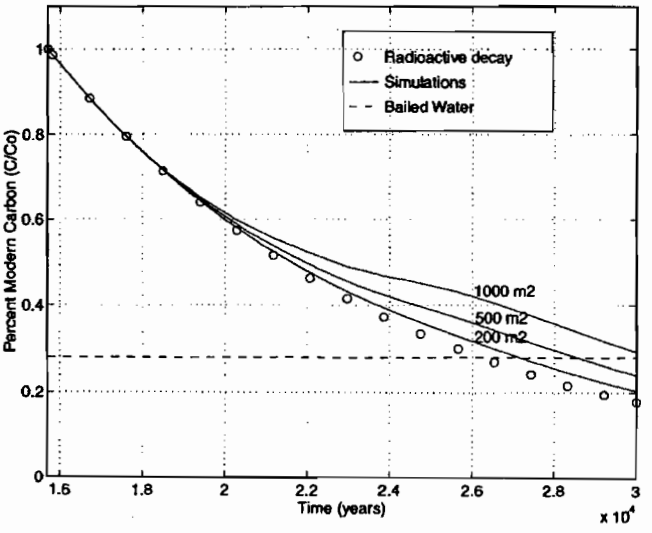

Figure 17. Depletion of perched water ^{14}C as a function of time for $q = 0.13$ mm/yr and three areal extent values. LHS-generated hydrologic properties are used.

function of time for each material property realization and also for a set of three values for the areal extent parameter A. Also shown in Figures 15, 16, and 17 is the reference simulation, which corresponds to pure radioactive decay, and the target value of $PMC_{pres} = 0.28$. Several observations can be made from these figures. First, the $q = 6.2$ mm/yr simulation, using mean TSPA-93 values, could reach the target PMC_{pres} after a residence time between 10,000 and 20,000 years for realistic areal extent values (Figure 15). This timeframe is consistent with the time required for the volume to reach a $dV/dt = 0$ and also with the change of the climate around 18 to 20 kaBP (last pluvial). On the basis of the ^{14}C analysis alone, the $q = 0.51$ mm/yr simulation, using the entropy-fit mean TSPA-93 values, seems to be plausible, since it can reach the target PMC_{pres} for realistic areal extent values, that is, before 20,000 years (Figure 16). However, the hydrological constraints are violated for this simulation since the perched water volume is consistently much larger than the target volume, V_{pres}, during this timeframe and also because $dV/dt \neq 0$, indicating nonattainment of steady-state conditions. Finally, the $q = 0.13$ mm/yr simulation, using the LHS-generated random realization properties, appears to be violating both hydrological and geochemical constraints, since (1) it attains a $dV/dt = 0$ and $V = V_{pres}$ after 25,000 years, and (2) it reaches the target PMC_{pres} after at least 30,000 years (Figure 17).

Conclusions

The major conclusions of this study are:

1. a fault-induced perched water trap model, postulated in the first part of this two-part paper (Bagtzoglou, 2002), has been proven plausible based on a fair correlation between areas of high potential recharge, location of significant structural features (e.g., faults), and known occurrences of perched water at YM;
2. a sustainable perched water body can be attained with an average deep recharge rate of 0.13, 0.51, and 6.2 mm/yr depending on the hydrologic properties of the rock units involved in the analyses;
3. only one of the three realizations tested (the one corresponding to recharge of 6.2 mm/yr) was able to satisfy both hydrological and geochemical constraints, given several key assumptions. This is in excellent agreement with the works of Stothoff et al. (1995), Stothoff (1997), and Bodvarsson et al. (1999), who predicted net infiltration rates in the range of 3 to 35 mm/yr with an average of 14 mm/yr, and 2 to 20 mm/yr with an average of 5 mm/yr, respectively. Very recently, Buscheck et al. (2002) have provided an estimate of 6 mm/yr for the average infiltration rate. This clearly demonstrates the reasonable discriminatory power of the proposed approach, which can readily be applied to any other site; and
4. it appears that for the realization that satisfies both hydrological and geochemical constraints, a present-day perched water body that consists of a combination of some minimal relict (past pluvial) water and young water from infiltration is an appropriate hypothesis. This is also in excellent agreement with observed data and the current conceptual model of flow and transport at YM (Wu et al., 1999).

Acknowledgements

This paper was prepared to document in part work performed by the author during his tenure at the Center for Nuclear Waste Regulatory Analyses (CNWRA) for the Nuclear Regulatory Commission (NRC) under Contract No. NRC-02-93-005. The activities reported here were performed on behalf of the NRC Office of Nuclear Material Safety and Safeguards, Division of Waste Management, and the NRC Office of Nuclear Regulatory Research, Division of Regulatory Applications. The paper is an independent product and does not necessarily reflect the views or regulatory position of the NRC. The numerical codes BIGFLOW and BREATH used in this work are configured under CNWRA's Software Configuration Procedure. The author thanks Mr. T. L. Tolley and Drs. S. A. Stothoff and D. R. Turner for their collaboration and support during the early part of this study. Drs. G. Ofoegbu and B. Sagar provided technical and programmatic reviews of a preliminary version of this paper, which helped improve its quality. Finally, the author acknowledges the thorough and constructive reviews received by the three anonymous referees and the editorial staff of the journal.

References

Bagtzoglou, A. C. 2003. Perched water bodies in arid environments and their role as hydrologic constraints for recharge rate estimation: A modeling methodology. *Environmental Forensics* 4(1):39–46.

Bish, D. L., and Aronson, J. L. 1993. Paleogeothermal and paleohydrologic conditions in silicic tuff from Yucca Mountain, Nevada. *Clays and Clay Minerals* 41:148–161.

Bish, D. L., and Chipera, S. J. 1989. *Revised Mineralogic Summary of Yucca Mountain, Nevada.* LA-11497-MS. Los Alamos, NM: Los Alamos National Laboratory.

Bodvarsson, G. S., Boyle, W., Patterson, R., and Williams, D. 1999. Overview of scientific investigations at Yucca Mountain—the potential repository for high-level nuclear waste. *Journal of Contaminant Hydrology* 38:3–24.

Broxton, D. E., Chipera, S. J., Byers, F. M., Jr., and Rautman, C. A. 1993. *Geologic Evaluation of Six Nonwelded Tuff Sites in the Vicinity of Yucca Mountain, Nevada for a Surface-Based Test Facility for the Yucca Mountain Project.* LA-12542-MS UC-814. Los Alamos, NM: Los Alamos National Laboratory.

Burger, P., and Scofield, K. 1994. Perched water at Yucca Mountain and their implications on the Exploratory Studies Facility. *EOS, Transactions, American Geophysical Union.* 75(44):250.

Buscheck, T. A., Rosenberg, N. D., Gansemer, J., and Sun, Y. 2002. Thermohydrologic behavior at an underground nuclear waste repository. *Water Resources Research* 38(3):10-1–10-19.

Byers, F. M., Jr., Carr, W. J., and Orkild, P. P. 1989. Volcanic Centers of Southwestern Nevada: Evolution of Understanding, 1960–1988. *Journal of Geophysics Research* 94(B5):5908–5924.

Craig, R. W., and Reed, R. L. 1991. *Geohydrology of Rocks Penetrated by Test Well USW H-6, Yucca Mountain, Nye County, Nevada.* USGS Water-Resources Investigations Report 89–4025. Denver, CO: US Geological Survey.

Czarnecki, J. B. 1985. *Simulated Effects of Increased Recharge on the Ground-Water Flow System of Yucca Mountain and Vicinity,*

Nevada-California. USGS Water-Resources Investigations Report 84-4344. Denver, CO: US Geological Survey.

Dohrenwend, J. C. 1987. *Basin and Range*. In *Geomorphic Systems of North America: Boulder, Colorado*, edited by W. L. Graf. Geological Society of America. Centennial Special Volume 2.

Fabryka-Martin, J. T., Dixon, P. R., Levy, S., Liu, B., Turin, H. J., and Wolfsberg, A. V. 1996. *Systematic Sampling for Chlorine-36 in the Exploratory Studies Facility*. LA-CST-TIP-96-001. Los Alamos, NM: Los Alamos National Laboratory.

Fiero, B. 1986. *Geology of the Great Basin*. Reno, NV: University of Nevada Press.

Flint, L. E., and Flint, A. L. 1990. *Preliminary Permeability and Water-Retention Data for Nonwelded and Bedded Tuff Samples, Yucca Mountain Area, Nye County, Nevada*. US Geological Survey Open-File Report 90-569. Denver, CO: US Geological Survey.

Flint, A. L., and Flint, L. E. 1994. Spatial distribution of potential near surface moisture flux at Yucca Mountain. *Proceedings of the Fifth Annual International Conference on High Level Radioactive Waste Management*. La Grange Park, IL: American Nuclear Society. pp. 2352–2358.

Flint, L. E., Flint, A. L., Moyer, T. C., and Geslin, J. K. 1995. Lateral Diversion of Water in the Paintbrush Tuff Nonwelded Hydrologic Unit, Yucca Mountain, Nevada. *EOS, Transactions, American Geophysical Union*. 76(46):F182.

Frizzell, V. A., Jr., and Shulters, J. 1990. *Geologic Map of the Nevada Test Site, Southern Nevada. 1:100,000*. US Geological Survey Miscellaneous Investigations Series Map I-2046.

Freeze, A. R., and Cherry, J. A. 1979. *Groundwater*. Englewood Cliffs, NJ: Prentice-Hall.

Geyh, M. A., Froehlich, E., and Verhagen, B. Th. 1995. Isotope hydrogeology and water balance assessment near the Nile in Sudan. *Application of Tracers in Arid Zone Hydrology* 232:57–66.

Hevesi, J. A., Istok, J. D., and Flint, A. L. 1992a. Precipitation estimation in mountainous terrain using multivariate geostatistics. Part I: Structural analysis. *Journal of Applied Meteorology* 31(7):661–676.

Hevesi, J. A., Flint, A. L., and Istok, J. D. 1992b. Precipitation estimation in mountainous terrain using multivariate geostatistics. Part II: Isohyetal Maps. *Journal of Applied Meteorology* 31(7):677–688.

Hevesi, J. A., Ambos, D. S., and Flint, A. L. 1994. A preliminary characterization of the spatial variability of precipitation at Yucca Mountain, Nevada. *Proceedings of the Fifth International High Level Radioactive Waste Management Conference*. La Grange Park, IL: American Nuclear Society. pp. 2520–2529.

Iman, R. L., and Shortencarier, M. J. 1984. *A FORTRAN 77 Program and User's Guide for the Generation of Latin Hypercube and Random Samples for Use with Computer Models*. Albuquerque, NM: Sandia National Laboratories.

Istok, J. D., Rautman, C. A., Flint, L. E., and Flint, A. L. 1994. Spatial variability in hydrologic properties of a volcanic tuff. *Ground Water* 32(5):751–760.

Loscot, C. L., and Hammermeister, D. P. 1992. *Geohydrologic Data from Test Holes UE-25 UZ#4 and UE-25 UZ#5, Yucca Mountain Area, Nye County, Nevada*. USGS Open-File Report 90-369. Denver, CO: US Geological Survey.

National Climatic Data Center. (1994) *WBAN Hourly Surface Observations*. March 1984 through February 1994. Asheville, NC: National Oceanic and Atmospheric Administration.

Ofoegbu, G. I., Bagtzoglou, A. C., Green, R. T., and Muller, M. 1999. Effects of perched water on thermally driven moisture flow at the proposed Yucca Mountain repository for high-level waste. *Nuclear Technology* 125(2):235–253.

Ofoegbu, G. I., Painter, S., Chen, R., Fedors, R. W., and Ferrill, D. A. 2001. Geomechanical and thermal effects on moisture flow at the proposed Yucca Mountain nuclear waste repository. *Nuclear Technology* 134(3):241–262.

Quade, J., and Mifflin, M. 1995. Fossil spring deposits in the southern Great Basin and their implications for changes in water-table levels near Yucca Mountain, Nevada, during Quaternary time. *Geological Society of America Bulletin* 107(2):213–230.

Russell, C., Hess, J., and Tyler, S. 1987. Hydrogeologic investigations of flow in fractured tuffs, Rainier Mesa, Nevada Test Site. *Flow and Transport Through Unsaturated Fractured Rock*, edited by D. D. Evans and T. J. Nicholson. Geophysical Monograph 42. Washington, DC: American Geophysical Union. pp. 43–50.

Scott, R. B., and Bonk, J. 1984. *Preliminary Geologic Map (1:12,000 scale) of Yucca Mountain, Nye County, Nevada, with Geologic Cross Sections*. USGS Open-File Report 84-494. Denver, CO: US Geological Survey.

Spaulding, W. G. 1985. *Vegetation and Climates of the Last 45,000 Years in the Vicinity of the Nevada Test Site, South-Central Nevada*. US Geological Survey Professional Paper 1329. Washington, DC: US Government Printing Office.

Stewart, J. H. 1984. Basin-Range Structure in Western North America: A Review. *Cenozoic Tectonics and Regional Geophysics of the Western Cordillera*. Memoir 152. Boulder, CO: The Geophysical Society of America.

Stirewalt, G., Henderson, B., and Young, S. 1994. *A Preliminary Three-Dimensional Geological Framework Model for Yucca Mountain, Nevada: Report to Accompany Model Transfer to the Nuclear Regulatory Commission*. CNWRA 94-023. San Antonio, TX: Center for Nuclear Regulatory Analyses.

Stirewalt, G. L., and Henderson, D. B. 1995. A preliminary three-dimensional geological framework model for Yucca Mountain. *Proceedings of the Sixth International Conference on High Level Radioactive Waste Management*. La Grange Park, IL: American Nuclear Society. pp. 116–118.

Stothoff, S. 1995. *BREATH Version 1.1-Coupled Flow and Energy Transport in Porous Media: Simulator Description and User Guide*. NUREG-CR 6333. Washington, DC: Nuclear Regulatory Commission.

Stothoff, S. A. 1997. Sensitivity of long-term bare soil infiltration simulations to hydraulic properties in an arid environment. *Water Resources Research* 33(4):547–558.

Stothoff, S. A., Bagtzoglou, A. C., and Castellaw, H. M. 1995. Estimation of spatial distribution of recharge factors at Yucca Mountain. In *NRC High-Level Radioactive Waste Research at CNWRA: January-June 1995*, edited B. Sagar. CNWRA 95-01S. San Antonio, TX: Center for Nuclear Waste Regulatory Analyses. pp. 9-5–9-12.

Thordarson, W. 1965. *Perched Ground Water in Zeolitized-Bedded Tuff, Rainier Mesa and Vicinity, Nevada Test Site, Nevada*. US Geological Survey Open-File Report TEI-862.

US Department of Energy (DOE). 1986. *Final Environmental Assessment: Yucca Mountain Site, Nevada Research and Development Area, Nevada*. DOE/RW-0073. Washington, DC: US Department of Energy.

US Department of Energy (DOE). 1988. *Site Characterization Plan, Yucca Mountain Site, Nevada Research and Development Area, Nevada*. DOE/RW-0199. Washington, DC: US Department of Energy.

US Department of Energy (DOE). 1992. *Report of Early Site Suitability Evaluation of the Potential Repository Site at Yucca Mountain, Nevada*. Washington, DC: US Department of Energy.

Wang, J. S. Y., Cook, N. G. W., Wollenberg, H. A., Carnahan, C. L., Javandel, I., and Tsang, C. F. 1993. Geohydrologic data and models of Rainier Mesa and their implications to Yucca Mountain. *Proceedings of the Fourth International Conference on High Level Radioactive Waste Management*. La Grange Park, IL: American Nuclear Society. pp. 675–680.

Whitfield, M. S., Cope, C. M., and Loscot, C. L. 1993. *Borehole and Geohydrologic Data for Test Hole USW UZ-6, Yucca Mountain Area, Nye County, Nevada*. USGS Open-File Report 92-28. Denver, CO: US Geological Survey.

Wilson, M. L., Gauthier, J. H., Barnard, R. W., Barr, G. E., Dockery, H. A., Dunn, E., Eaton, R. R., Guerin, D. C., Lu, N., Martinez, M. J., Nilson, R., Rautman, C. A., Robey, T. H., Ross, B., Ryder, E. E., Schenker, A. R., Shannon, S. A., Skinner, L. H., Halsey, W. G., Gansemer, J. D., Lewis, L. C., Lamont, A. D., Triay, I. R., Meijer, A., and Morris, D. E. 1994. *Total-System Performance Assessment for Yucca Mountain—SNL Second Iteration (TSPA-1993)*. SAND93-2675. Albuquerque, NM: Sandia National Laboratories.

Wood, W. W., and Sanford, W. E. 1995. Chemical and isotopic methods for quantifying groundwater recharge in a regional, semiarid environment. *Ground Water* 33(3):458–468.

Wu, Y. S., Ritcey, A. C., and Bodvarsson, G. S. 1999. A modeling study of perched water phenomena in the unsaturated zone at Yucca Mountain. *Journal of Contaminant Hydrology* 38:157–184.

Yang, I. C., Rattray, G. W., and Yu, P. 1996. *Interpretations of Chemical and Isotopic Data from Boreholes in the Unsaturated Zone at Yucca Mountain, Nevada.* US Geological Survey Water-Resources Investigations Report 96-4058.

Young, S. R., Stirewalt, G. L., and Morris, A. P. 1992. *Geometric Models of Faulting at Yucca Mountain.* CNWRA 92-008. San Antonio, TX: Center for Nuclear Waste Regulatory Analyses.